

Emergence of material momentum in optical media

Deng Pan,^{1*} Hongxing Xu² and F. Javier García de Abajo^{1,3}

¹ ICFO-Institut de Ciències Fotoniques, The Barcelona Institute of Science and Technology, 08860 Castelldefels (Barcelona), Spain.

² School of Physics and Technology, Wuhan University, Wuhan 430072, China.

³ ICREA-Institució Catalana de Recerca i Estudis Avançats, Passeig Lluís Companys 23, 08010 Barcelona, Spain.

In the standard description of light propagation through a nonmagnetic medium—a solution of Maxwell’s equations incorporating the frequency-dependent dielectric permittivity $\varepsilon(\omega)$ —photons are just accompanied by an alternating-current (AC) density wave. From a classical perspective, the latter is formed by electrons oscillating around their equilibrium positions, so it does not possess a net momentum. Here, we show that quantum mechanics predicts instead a net momentum associated with the AC current-density wave, which manifests in the emergence of an electric direct current (DC). Unveiling this momentum allows us to unambiguously resolve the century-old controversy on the photon momentum inside a medium. The quantum model further enables us to explicitly calculate the ratio of momentum distributed in matter and electromagnetic fields for relevant types of classical media and even in materials supporting unconventional quantum states. Our findings provide fundamental new understanding on the behavior of light and photon-coupled polaritons in material media.

Despite the celebrated success of Maxwell’s equations in predicting the behavior of light in different scenarios, the remaining fundamental controversy on the light momentum in a medium is still perplexing. The photon momentum in vacuum, $\hbar q_0$, is well established in terms of the wave vector $q_0 = \omega/c$. The problem arises when trying to determine the momentum of a photon propagating in a medium of refractive index n . Two possible solutions, $n\hbar q_0$ and $\hbar q_0/n$, were proposed by Minkowski (1) and Abraham (2), respectively, shortly after the formulation of Maxwell’s equations, giving birth to a controversy that has been the subject of heated debate for over 100 years, from both theoretical (3–13) and experimental (14–21) perspectives. Theoretical considerations are mainly based on examination of Maxwell’s equations, without in-depth consideration of the microscopic response of the medium, resulting in two mutually-contradictory, yet internally self-consistent formalisms within the framework of Maxwell’s equations. The Abraham–Minkowski (AM) controversy refers to the partition of momentum be-

tween field and matter in the interaction of light with macroscopic media. Recent studies speculate that the Abraham form stands for the momentum of the electromagnetic (EM) field (10), while a momentum in matter is elusive from the perspective of Maxwell’s equations and seems to be at odds with a classical perception, as provided for example by the Drude model, in which the charges are only found to harmonically oscillate around their equilibrium positions.

At a microscopic level, the momentum of photons is well understood in quantum theory, and in fact the law of momentum conservation governs all phenomena involving the interaction between photons and elementary particles, such as the photoelectric effect and Compton scattering. Momentum transfer also takes place in the photogalvanic effect, in which incident photons with energy lower than the work function of the material generate an internal photoelectric effect that results in an electric direct current (DC). This photogalvanic effect has been extensively studied in semiconductors (22–25) and explained in terms of interband electron-hole pair excitations, while we note here that such DC current generation is in fact a general phenomenon occurring during

*Electronic address: deng.pan@icfo.eu

light-medium interaction; for example, oblique light incident on a thin metallic film or graphene also gives rise to a DC current by transfer of momentum to conduction electrons (26, 27). The understanding of these photoexcited DC currents is straightforward from the perspective of momentum conservation between quantized photons and electrons, but it cannot be explained only from Maxwell's equations simply because a DC current cannot be driven by the alternating electric field of monochromatic light. We argue that a full understanding of the momentum of photons propagating inside a medium, as well as that of states involving photons coupled to polaritons, requires us to consider the interactions between photons and a large number of charged particles in the materials, which can only be accomplished by accounting for the quantum nature of the optical media beyond the classical description provided by the refractive index $n(\omega)$ in the Maxwell equations.

Here, following a simple, yet unambiguous analysis based on fundamental aspects of quantum mechanics we show that the momentum of photons propagating in a medium is intrinsically associated with a component contained in the medium, which manifests as an electric DC current even in the absence of inelastic damping, arising from a similar mechanism as the photogalvanic effect. Through this analysis, we bridge the quantum description of optical media and Maxwell's equations, thus allowing us to explicitly calculate the ratio of momentum distributed in matter and the EM field. Our results confirm that, within the local response limit for both transverse EM waves propagating in a homogeneous medium and longitudinal waves such as plasmons in a 2D electron gas (2DEG) or graphene, the momentum distribution is in good agreement with the AM formalism; if nonlocal effects become important, particularly when the system supports strongly confined modes, such as acoustic plasmons in bilayer graphene, a substantially larger fraction of momentum is placed in the medium than predicted by the classical estimate. Our results pave the way to understand momentum in photon-coupled polariton states sustained by both conventional and nonclassical materials.

Results

Quantum description of optical media. Two typical scenarios for light propagation in optical media are shown in Fig. 1: a plasmon polariton wave sustained by a 2DEG (Fig. 1a), and a transverse EM plane wave prop-

agating in a 3D bulk transparent dielectric medium (Fig. 1b). In this study, we restrict our discussions to steady states of light propagating in infinitely extended systems. According to Maxwell's equations, in both scenarios, when only monochromatic light is involved, the time-harmonic electric field $\mathbf{E}(\omega)$ induces a distribution of polarization vector $\mathbf{P}(\omega) = \chi(\omega)\mathbf{E}(\omega)$ dictated by the material's electric susceptibility $\chi(\omega)$, which consequently generates an alternating-current (AC) polarization density wave $\mathbf{J}_{AC}(\omega) = \partial_t\mathbf{P}(\omega)$. This wave is longitudinal in 2D plasmons and transverse in EM waves in a dielectric (black arrows and curves in Fig. 1a,b). Additionally, the longitudinal $\mathbf{J}_{AC}(\omega)$ current in 2D plasmons gives rise to a charge-density wave via charge continuity (color scale, Fig. 1a). The current-density wave $\mathbf{J}_{AC}(\omega)$ and the material's electric susceptibility $\chi(\omega)$ comprise the whole description of optical media in the framework of Maxwell's equations.

In the realm of quantum theory, the formation of AC current-density waves $\mathbf{J}_{AC}(\omega)$ is the result of the photoexcited transitions among electron states in momentum space, as illustrated in Fig. 1c (examples of states in real space are shown by dashed curves in Fig. 1a). From the analysis presented below, we also conclude that those transitions inherently generate DC currents (red arrows in Fig. 1a,b), which account for the fraction of momentum distributed in the medium. A photon propagating inside a medium containing Bloch electrons is a coupled state described by a Hamiltonian $\hat{H}_p + e(\hat{\mathbf{p}} \cdot \mathbf{A} + \mathbf{A} \cdot \hat{\mathbf{p}})/2m_e + \hat{\mathbf{p}}^2/2m_e - eV(\mathbf{r})$, where terms from left to right stand for the energy of the free EM field, the light-matter interaction and the electrons in a model periodic ionic potential $V(\mathbf{r})$. The electron states are Bloch waves defined as eigenfunctions of $\hat{\mathbf{p}}^2/2m_e - eV(r)$, namely $\psi_{j\mathbf{k}} = e^{i\mathbf{k}\cdot\mathbf{r}}u_{j\mathbf{k}}(\mathbf{r})/\sqrt{\nu}$, where ν is a normalization volume in 3D or area in 2D, \mathbf{k} is the Bloch wave vector, and $u_{j\mathbf{k}}(\mathbf{r})$ is a normalized function with the same periodicity as the atomic lattice. Under the perturbation described by the minimal light-electrons coupling term $e(\hat{\mathbf{p}} \cdot \mathbf{A} + \mathbf{A} \cdot \hat{\mathbf{p}})/2m_e$, quantum transitions among electron states (color-filled circles in Fig. 1a,c) give rise to superposition wave functions $\Psi(\mathbf{r}, t) = c_1\psi_{j\mathbf{k}_1} + c_2\psi_{j'\mathbf{k}_2}e^{-i\omega t}$. The electric current density described by $\Psi(\mathbf{r}, t)$ is easily evaluated as $\mathbf{j} = -e\text{Re}\{\Psi^*\hat{\mathbf{p}}\Psi\}/m_e$, which gives rise to AC and

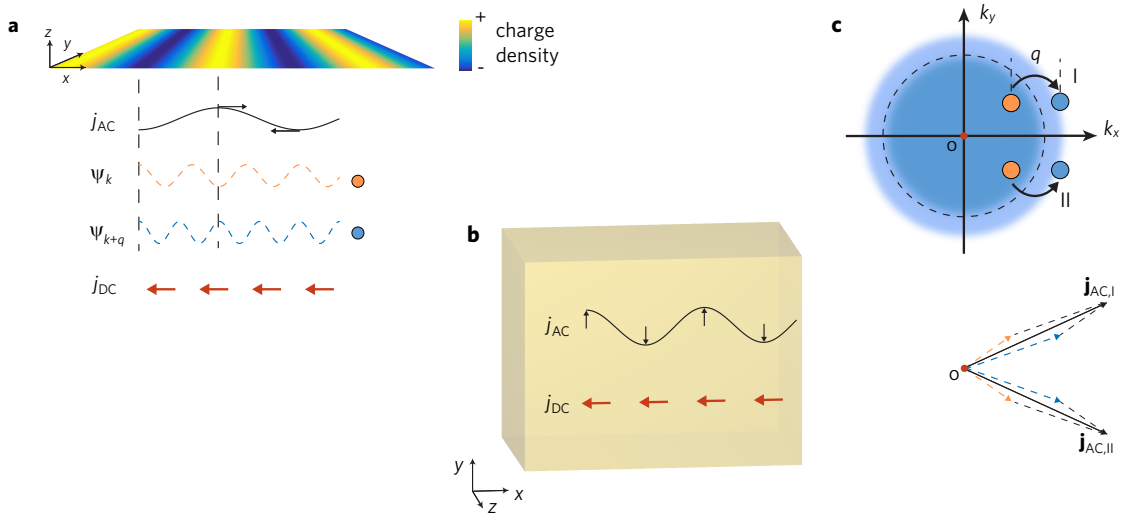


Fig. 1 Illustration of light propagation in optical media. **a,b** Plasmons on a 2DEG (**a**) and photons in a bulk dielectric medium (**b**) support longitudinal and transverse AC current-density waves (black curves and arrows), respectively. In both scenarios the media carry a momentum that manifests in the emergence of DC currents (red arrows). **c**, Photons propagating in a material are coupled states formed by the EM field combined with electronic quantum transitions between states denoted by color-filled circles in the momentum space representation of the upper panel. The optical wave vector \mathbf{q} is assumed to be along \hat{x} . The transitions I and II produce AC current waves $\mathbf{j}_{AC,I}$ and $\mathbf{j}_{AC,II}$ (see Eq. (1)) whose directions are shown by black arrows in the bottom panel. The in-phase and out-of-phase superpositions of $\mathbf{j}_{AC,I}$ and $\mathbf{j}_{AC,II}$ transition currents result in the total longitudinal and transverse AC current-density perturbances observed in plasmons (**a**) and transverse EM waves (**b**). In plasmons, the charge-density waves (color scale in **a**) are formed by the quantum superposition of pairs of electronic quantum states ψ_k and ψ_{k+q} of momenta k and $k + q$ (dashed curves); for illustration purposes both momenta are assumed to be along \hat{x}). The resulting real-space charge-density $-e|\Psi(x, t)|^2$ is presented in the color scale. During the transitions shown in **c**, the medium also gains a net momentum, as revealed by an emerging DC electric current (see Eq. (2)).

DC components

$$\mathbf{j}_{AC} \approx \frac{-e}{\nu m_e} \text{Re}\{c_1^* c_2 e^{i(\mathbf{q}\cdot\mathbf{r}-\omega t)}\} \hbar(\mathbf{k}_1 + \mathbf{k}_2), \quad (1)$$

$$\mathbf{j}_{DC} = \frac{-e}{\nu m_e} \left(|c_1|^2 \langle \hat{\mathbf{p}} \rangle_{j\mathbf{k}_1} + |c_2|^2 \langle \hat{\mathbf{p}} \rangle_{j'\mathbf{k}_2} \right), \quad (2)$$

respectively. The approximation in Eq. (1) is made for nearly free electrons, but the discussions below have general validity for rigorous solutions. The AC current (Eq. (1)) is a propagating wave characterized by a wave vector $\mathbf{q} = \mathbf{k}_2 - \mathbf{k}_1$ (we take $\mathbf{q} = q\hat{x}$ throughout this paper), while the current direction is aligned with the sum of momenta of initial and final electron states $\mathbf{k}_1 + \mathbf{k}_2$ (see bottom panel in Fig. 1c). The DC currents, which is proportional to the total momentum of the electron, receives contributions from each Bloch state, $\langle \hat{\mathbf{p}} \rangle_{j\mathbf{k}_i} = \langle \psi_{j\mathbf{k}_i} | \hat{\mathbf{p}} | \psi_{j\mathbf{k}_i} \rangle$.

The polarization current-density waves $\mathbf{J}_{AC}(\omega)$ entering the Maxwell equations must result from the sum

of the AC current waves in Eq. (1) for all possible transitions in \mathbf{k} -space (Fig. 1c). For the plasmons and transverse EM waves considered in Fig. 1a,b, where the electric field is parallel and perpendicular to \mathbf{q} , respectively, the AC currents in Eq. (1) produced by two transitions symmetrically distributed in \mathbf{k} -space ($\mathbf{j}_{AC,I}$ and $\mathbf{j}_{AC,II}$ in Fig. 1c) are in-phase or out-of-phase, so that the total current-density waves $\mathbf{J}_{AC}(\omega)$ are longitudinal or transverse, respectively. In addition, the charge-density wave in the plasmons can also be understood as a quantum superposition, as illustrated in Fig. 1a by considering two quantum states with $\mathbf{k}_{1,2}$ both along \hat{x} (dashed curves, Fig. 1a), where the charge density appears as a propagating wave $-e|\Psi(x, t)|^2 = -2e\text{Re}\{c_1^* c_2 e^{i(qx-\omega t)}\}/\nu$ (Fig. 1a, blue solid curve). The polarization current-density turns out to be proportional to the optical electric field, and we can write $\mathbf{J}_{AC} = \omega^2 \chi(\omega) \mathbf{E}(\omega)$, which defines the electric susceptibility $\chi(\omega)$ of the optical medium. This procedure reproduces the well-

established result (28)

$$\chi_{T,L}(\mathbf{q}, \omega) = -\frac{\omega_p^2}{\omega^2} - \frac{\omega_p^2}{\omega^2} \frac{2\hbar}{Nm_e} \times \sum_{jj', \mathbf{k}} |K_{T,L}|^2 \frac{f_{j\mathbf{k}} - f_{j'\mathbf{k}+\mathbf{q}}}{\omega - \omega_{j'\mathbf{k}+\mathbf{q}} + \omega_{j\mathbf{k}} + i\gamma}, \quad (3)$$

where we include the contribution of the paramagnetic current in first term, $\omega_p = \sqrt{Ne^2/\nu\epsilon_0 m_e}$ is the plasmon frequency, N is total number of charge carriers, K_T and K_L are transverse components of transition matrix elements $\mathbf{K} = \langle u_{j\mathbf{k}} | \mathbf{k} + \mathbf{q}/2 - i\nabla | u_{j'\mathbf{k}+\mathbf{q}} \rangle$, $f_{j\mathbf{k}}$ and $\hbar\omega_{j\mathbf{k}}$ are the population and energy of the electron state with wave vector \mathbf{k} and band index j , and γ is a small phenomenological damping rate of the material. In the local limit ($q \rightarrow 0$), the contributions of intra- and interband transitions reduce to the Drude model and Lorentz model (29), respectively.

DC current associated with propagating light. Equations (1) and (3) constitute the standard description of nonmagnetic optical media in a quantum approach, which reduces the AC response to an electric susceptibility that enters Maxwell's equations. However, the DC current in Eq. (2) is not present in Maxwell's equations, and we show here that it is precisely this DC current what can help us to fully understand the momentum partition of photons in a medium. To this end, we find the nonvanishing total DC current \mathbf{J}_{DC} by summing Eq. (2) over all possible transitions, and consequently the total momentum in the medium is determined by the relation $\mathbf{g}_{ele} = -m_e \mathbf{J}_{DC}/e$. We find

$$\mathbf{g}_{ele} = \frac{e^2 |E_i|^2}{2\omega^2 m_e^2 \nu} \sum_{jj', \mathbf{k}} |K_{T,L}|^2 (\langle \hat{\mathbf{p}} \rangle_{j'\mathbf{k}+\mathbf{q}} - \langle \hat{\mathbf{p}} \rangle_{j\mathbf{k}}) \times \frac{f_{j\mathbf{k}} - f_{j'\mathbf{k}+\mathbf{q}}}{|\omega - \omega_{j'\mathbf{k}+\mathbf{q}} + \omega_{j\mathbf{k}} + i\gamma|^2}, \quad (4)$$

where $i = y$ for T and $i = x$ for L. We observe that \mathbf{J}_{DC} arises due to the intrinsic momentum distributed among the electrons. Although Eq. (4) is quadratic in the electric field, we note that it is not an ordinary optical nonlinear effect (30), and therefore, it cannot be simply incorporated into Maxwell's equations through higher-order susceptibility components $\chi^{(2)}, \dots$ obtained from higher-order quantum perturbation theory. In particular, this DC current should not be confused with the optical rectification effect, which results in a distribution of permanent dipole moments in a steady state.

We conclude from Eq. (4) that the DC current here revealed is a universal intrinsic phenomenon of light prop-

agation in a medium, regardless of the light frequency and conductivity properties of the material. For free electron systems, such as plasmonic thin metal films (illustrated in Fig. 1a) or graphene, a DC current associated with the plasmons has been experimentally confirmed (27). For an insulating medium with its Fermi energy located in the bandgap, as illustrated by the two lowest bands calculated in the Kronig-Penney model (31) in Fig. 2a (see periodic potential in the inset), the optical response receives contributions from interband transitions. A well-known photogalvanic effect takes place when the photon energy exceeds the bandgap energy $\hbar\omega > E_g$, so that the electrons are continuously excited to the conduction band, giving rise to a DC current. When the medium sustains the photogalvanic effect, it is strongly absorptive, as indicated by the singularity of Eq. (4) in the $\gamma \rightarrow 0$ limit for $\omega = \omega_{j'\mathbf{k}+\mathbf{q}} - \omega_{j\mathbf{k}}$ with $j \neq j'$ (we note that a dissipation mechanism is indispensable to avoid a constant increase in the population of the conduction electron band). Rather unexpectedly, Eq. (4) also predicts the presence of a DC current in lossless transparent media, since in the low damping limit $\gamma \rightarrow 0$ and for photon energy $\hbar\omega < E_g$ Eq. (4) converges to a nonzero value. The fact that this DC current results from interband transitions seems to be at odds with the assumption $\hbar\omega < E_g$. However, one must keep in mind that the conduction band also contributes to the optical response when $\hbar\omega < E_g$ (i.e., without inclusion of polarization due to interband transitions, light propagation is simply not affected by the medium, implying the unphysical result $\chi(\omega) = 0$ and $n(\omega) = 1$ inside any transparent material). The process of light propagation in a transparent medium can be explained as follows: interband transitions are initially produced under light excitation due to small fluctuations (small but nonzero γ), and after a considerable long period of time ($1/\gamma$) the electron population in the conduction band reaches a steady-state distribution. In the steady state we are concerned with in this study, the quantum superposition of Bloch states across the band gap gives rise to a AC current wave in the time-harmonic Maxwell equations (Fig. 1b) and also to a DC current following the mechanism explained in Fig. 1.

Momentum distribution in transverse EM waves.

With the electron momentum given by Eq. (4), we can clearly explain the AM controversy for transverse EM waves (Fig. 1b) by explicitly calculating the ratio of momentum distributed in the EM field and matter. The momentum of the EM field is determined

by the Maxwell equations, which leads to $g_{EM} = E_y H_z / 2c^2 = \epsilon_0 E_y^2 / 2c$ (32). For a weakly absorptive (i.e., in the low damping limit $\gamma \approx 0$) free electron system, fulfilling $\langle \hat{\mathbf{p}} \rangle_{\mathbf{k}+\mathbf{q}} - \langle \hat{\mathbf{p}} \rangle_{\mathbf{k}} = \hbar \mathbf{q}$, by comparing Eqs. (3) and (4), we can readily write the ratio between g_{ele} and g_{EM} as a simple expression (see Methods),

$$\frac{g_{ele}}{g_{EM}} = \chi(\omega) + \frac{\omega}{2} \frac{d\chi(\omega)}{d\omega}. \quad (5)$$

According to Minkowski's expression, the momentum of an individual photon in an EM plane wave is $g_M = n_p \hbar q_0$, where $n_p(\omega) = \sqrt{1 + \chi(\omega)}$ is the phase index, and $\chi(\omega)$ is determined by Eq. (3). For a dispersive material, Abraham's form of the photon momentum is $g_A = \hbar q_0 / n_g$, where $n_g(\omega) = d(\omega n_p) / d\omega$ is the group index. Taking these relations into consideration, the ratio in Eq. (5) reduces to $g_{ele} / g_{EM} = (g_M - g_A) / g_A$, which unambiguously reveals that the Abraham form of the photon momentum only accounts for the EM field, while Minkowski's expression includes the momentum imparted to electrons, associated with a DC current, as show in Fig. 1b.

The analysis above, made for free electron systems, is also applicable to light propagation in insulating media involving interband transitions. To show this, we again adopt a 1D Kronig-Penney model for illustration, and the momenta of electrons $\langle \hat{p}_x \rangle_{j\mathbf{k}}$ in the two bands ($j = 1, 2$) in Fig. 2a are calculated and shown in Fig. 2b. The two transitions around $-k$ and k (black arrows in Fig. 2a) yield a total electron momentum in Eq. (4) similar to free electrons, as concluded from the following considerations: in the local limit ($q \rightarrow 0$), the energy difference between two states in Eq. (4) is approximately $\hbar(\omega_{2,k} - \omega_{1,k})$; the sum of momentum difference $\sum_{\pm} \langle \hat{p}_x \rangle_{2,\pm k + \frac{q}{2}} - \langle \hat{p}_x \rangle_{1,\pm k - \frac{q}{2}}$ (Fig. 2b, black arrows), using to the symmetry $\langle \hat{p}_x \rangle_{-k} = -\langle \hat{p}_x \rangle_k$, becomes equal to the change of momentum in an average function $\langle \hat{p}_x \rangle_k = (\langle \hat{p}_x \rangle_{1,k} + \langle \hat{p}_x \rangle_{2,k}) / 2$ (Fig. 2b, grey curve), namely $2(\langle \hat{p}_x \rangle_{k+\frac{q}{2}} - \langle \hat{p}_x \rangle_{k-\frac{q}{2}})$ (Fig. 2b, grey arrows), which results in a value of nearly $2\hbar q$ (noticing the slope of the grey curve in Fig. 2b); the contribution of transitions near $k = 0$ to Eq. (4) is negligible due to the large energy difference. This resemblance results from the time reversal symmetry $\langle \hat{\mathbf{p}} \rangle_{-k} = -\langle \hat{\mathbf{p}} \rangle_k$, which is therefore also valid for 3D media supporting transverse EM waves. Following these considerations, we conclude that in the local limit the momentum carried by the DC current associated with illuminated Bloch electrons also accounts for the difference between Abraham

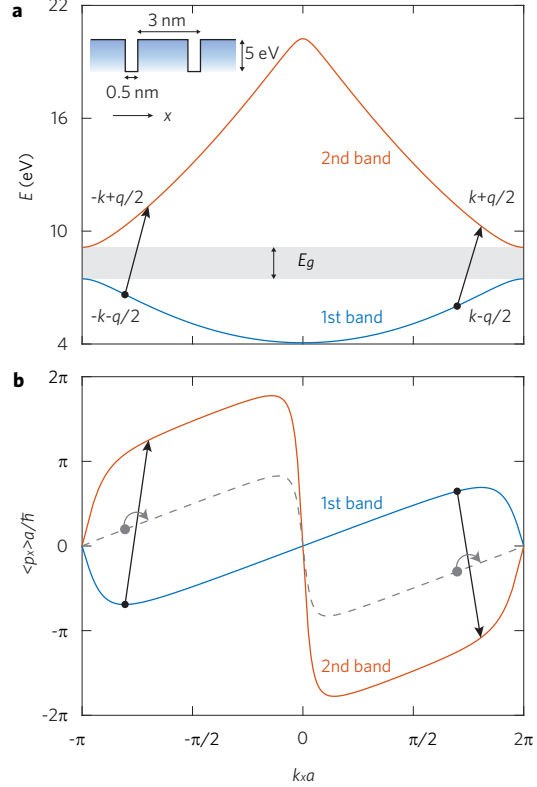


Fig. 2 Light excitations of electrons in a 1D periodic potential. **a**, Electron dispersion of the two lowest bands calculated for the periodic potential illustrated in the inset. **b**, Momentum of electrons in the two bands of **a**. In the local limit ($q \rightarrow 0$), considering transitions around k and $-k$ (black arrows in **a** and **b**), the sum of momentum changes can be equally represented by the momentum change in the dashed curves (grey arrows).

and Minkowski momenta.

Momentum of 2D plasmons. Equation (4) can also be applied to calculate the momentum distribution in the 2D plasmons shown in Fig. 1a. Results for the effective refractive index of the plasmon mode, defined by $n_{neff}(\omega) = qc/\omega$, are shown in Fig. 3a as calculated for free-standing 2DEGs of different electron densities based on the electric susceptibility in Eq. (3) (for $\gamma = 0$). The simplicity of the 2DEG system also allows us to easily calculate the momentum associated with the EM field g_{ele} by integrating $E_y H_z / 2c^2$ along \hat{z} . With the momentum in the electrons g_{ele} determined in our quantum theory by Eq. (4), we finally obtain the ratio g_{ele} / g_{EM} to characterize the momentum distribu-

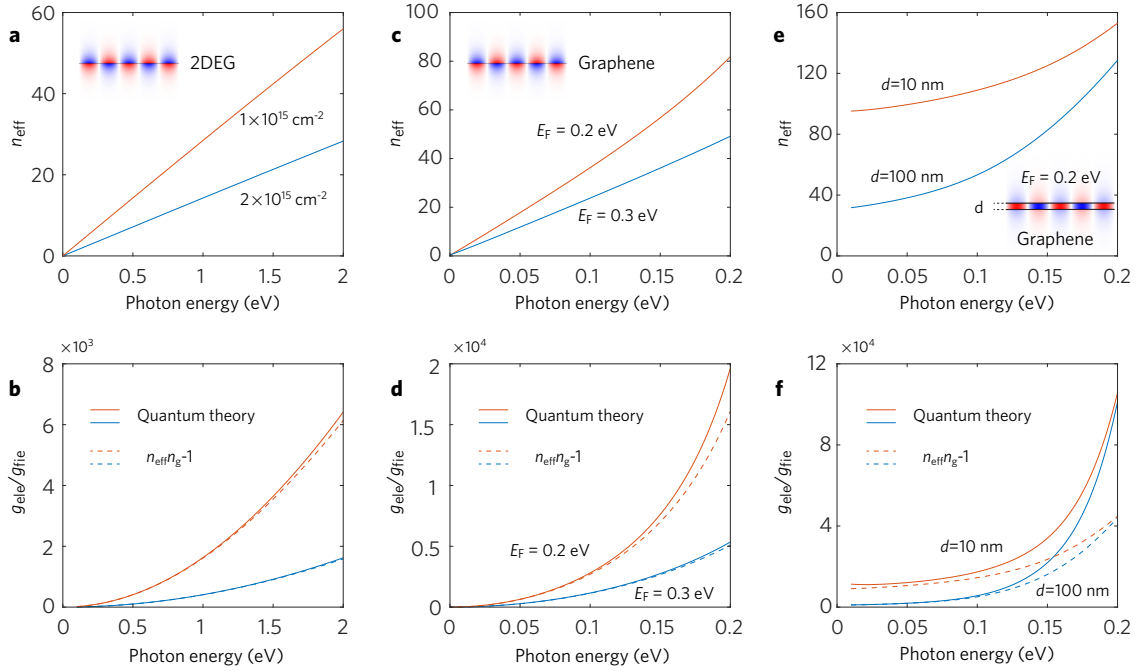


Fig. 3 Momentum distribution in plasmons. **a,b**, Effective refractive index (**a**) and momentum distribution (**b**) of plasmons in a freestanding 2DEG with two different carrier densities (see labels in **a**). In **b**, the ratios of momenta distributed in electrons and EM field are calculated based on our quantum model (solid curves) and compared with the classical estimate from the AM formalism (dashed curves). **c-f**, Same as **a** (**c,e**) and **b** (**d,f**) for monolayer (**c,d**) and bilayer (**e,f**) graphene. We show results for monolayer graphene with two different Fermi energies, and bilayer graphene with different separations.

tion in 2DEG plasmons. In Fig. 3b, we compare numerical results of $g_{\text{ele}}/g_{\text{EM}}$ (solid curves) with the estimate obtained from the AM formalism, $g_{\text{ele}}/g_{\text{EM}} = (g_{\text{M}} - g_{\text{A}})/g_{\text{A}} = n_{\text{eff}}n_{\text{g}} - 1$ (dashed curves), where the Minkowski momentum is defined as $g_{\text{M}} = n_{\text{eff}}\hbar\omega$, and the group index in the Abraham form $g_{\text{A}} = \hbar\omega/n_{\text{g}}$ is now $n_{\text{g}} = d(\omega n_{\text{eff}})/d\omega$.

As shown in Fig. 3b, the estimate given by the AM formalism is in good agreement with our quantum theory over a wide frequency range. In fact, we can analytically prove that in the local limit the electric susceptibility in Eq. (3) reduces to the Drude model and the electron momentum in Eq. (4) is exactly equivalent to the AM estimate $n_{\text{eff}}n_{\text{g}} - 1$. For higher frequencies, plasmons in the 2DEG show a large $n_{\text{eff}}(\omega)$ and strong confinement, where nonlocal corrections are not negligible (e.g., the plasmon wave vector q is no longer negligible compared with the Fermi wave vector k_{F}), and as a result the quantum theory here presented deviates from the AM estimate $n_{\text{eff}}n_{\text{g}} - 1$.

Our quantum model can also be generalized to investigate the momentum of graphene plasmons (33–36), whose large wave vector compared with vacuum photons produces strong nonlocal effects (37–39). The plasmon dispersion curves (Fig. 3c) and EM momentum g_{EM} in freestanding graphene can be obtained from the above equations for the 2DEG simply by using the electric susceptibility of graphene, which can be obtained in a similar way as Eq. (3). Additionally, the electron momentum g_{ele} in graphene, which is given by a similar expression to Eq. (4), involving intra- and inter-band transitions, is also associated with a DC electric current, which in fact has already been measured in experiment (27). We find the ratio $g_{\text{ele}}/g_{\text{EM}}$ obtained from this quantum model to be in good agreement with the AM estimate $n_{\text{eff}}n_{\text{g}} - 1$ (Fig. 3d), while deviations between them increase for higher photon energy and lower carrier density, where nonclassical effects are present due to the higher degree of field confinement (i.e., larger n_{eff} in Fig. 3c).

Quantum nonlocal effects can also be induced by geometry, such as in acoustic plasmons (38–41). The refractive index $n_{\text{eff}}(\omega)$ of acoustic plasmons supported by a bilayer graphene structure with a small separation d (see inset of Fig. 3e) is shown in Fig. 3e for different values of d . In the bilayer structure, the momentum of the field g_{EM} is obtained by integrating $E_y H_z / 2c^2$ over the three vacuum regions separated by the graphene layers, and the total electron momentum g_{ele} is obtained by summing the contributions of the two graphene layers. The ratio $g_{\text{ele}}/g_{\text{EM}}$ calculated from this quantum model is compared with the AM estimate $n_{\text{eff}}n_g - 1$ in Fig. 3f, where we observe considerable discrepancies at lower photon energy, which we attribute to the strong nonlocal effects in acoustic plasmons, as confirmed in experiments (38, 39). At higher photon energies close to E_{F} , the AM estimate $n_{\text{eff}}n_g - 1$ is only $\sim 50\%$ of the value obtained in the quantum model.

Discussion

To summarize, we have shown that the long-standing controversy on photon momentum in optical media originates in the overlook on a universal DC electric current that accounts for the photon momentum component associated with the medium. This DC current is unexpected from a classical perspective; it has a quantum origin, but it is a direct consequence of the classical oscillatory current associated with polarization in an illuminated medium, as described by Maxwell’s equations. The existence of this DC electric current is evidenced by a series of experimental observations, such as the photogalvanic effect in dielectric materials (22–25) (e.g., semiconductors) and metals (26, 27). In contrast to previously accepted results (18), our study confirms that the partition of the momentum of a photon propagating in a medium into light and matter components is not arbitrary; the material component is associated with a gauge-invariant DC current, and consequently, it could be measured through the resulting static magnetic field or electric voltage that it generates.

Our study also offers insights into the optical force acting on real object. In infinite systems, the optical force acting on the atomic lattice can only arise from the interaction with the photo-excited current, through electron-photon interactions in an ideally periodic potential or also via random elastic electron scattering events. In finite systems, the spatially nonuniform charges accumulated by the current can exert a force on

the atomic lattice via Coulomb interaction. A light pulse propagating in a material should also induce a DC current that is spatially nonuniform. When considering the coupling of electrons with the atomic lattice of the material, the pulse should induce local stress and compression in the medium. In addition, a DC current present in the polaritons sustained by a free-electron system excited by a localized source could cause a nonuniform electron distribution, such as in graphene plasmon generation assisted by a tip in SNOM measurements, and this electron nonuniformity could possibly lead to unexplored effects, such as a new dissipation mechanism.

Our study further reveals the existence of DC current loops when circularly polarized light or light beams carrying angular momentum are propagating in a medium. As a specific example, we claim the optical excitations on a small particle, such as localized plasmons on a nanosphere, to result from the superposition of internal quantum states with well-defined angular momentum, where the AC optical current leads to a circularly polarized electric dipole moment, and we predict an intrinsic DC current loop giving rise to a static magnetic field. This is in fact the generalization of the inverse Faraday effect to a free-electron system, and according to our theory a static magnetic field should instantaneously accompany the passage of a photon. This prediction should be testable in ultrafast time-resolved experiments.

Methods

Derivation of equation (5). For transverse EM waves, the derivative of the electric susceptibility for monochromatic light of frequency ω in Eq. (3) yields

$$\begin{aligned} \frac{\omega}{2} \frac{d\chi_{\text{T}}}{d\omega} &= \frac{\omega_{\text{P}}^2}{\omega^2} + \frac{\omega_{\text{P}}^2}{\omega^2} \frac{2\hbar}{\nu m_e} \times \\ &\quad \sum_{jj', \mathbf{k}} |K_{\text{T}}|^2 \frac{f_{j\mathbf{k}} - f_{j'\mathbf{k}+\mathbf{q}}}{\omega - \omega_{j'\mathbf{k}+\mathbf{q}} + \omega_{j\mathbf{k}} + i\gamma} \\ &\quad + \frac{\omega_{\text{P}}^2}{\omega} \frac{\hbar}{\nu m_e} \sum_{jj', \mathbf{k}} |K_{\text{T}}|^2 \frac{f_{j\mathbf{k}} - f_{j'\mathbf{k}+\mathbf{q}}}{(\omega - \omega_{j'\mathbf{k}+\mathbf{q}} + \omega_{j\mathbf{k}} + i\gamma)^2}, \end{aligned} \quad (6)$$

where the first two terms on the right-hand side are simply $-\chi_{\text{T}}(\mathbf{q}, \omega)$. For a free-electron system, the momentum change between states in Eq. (4) is $\langle \hat{\mathbf{p}} \rangle_{\mathbf{k}+\mathbf{q}} - \langle \hat{\mathbf{p}} \rangle_{\mathbf{k}} = \hbar\mathbf{q}$, and taking into account $g_{\text{EM}} = \varepsilon_0 E_y^2 / 2c$, the re-

maintaining third term in the above expression is equal to $g_{\text{ele}}/g_{\text{EM}}$, therefore proving Eq. (5).

Dispersions of 2D plasmons. The plasmon modes considered in the 2D electron systems in Fig. 3 are all transverse magnetic (TM) waves. For the 2D plasmons on a free-standing single-layer of 2DEG or graphene (Fig. 3a,c), all field components decay exponentially along the out-of-plane direction \hat{z} away from the film. The solution of Maxwell's equations consists of a combination of TM waves with in-plane wave vector q exceeding $k_0 = \omega/c$; as we are interested in self-sustained modes, the field can be constructed by including one evanescent wave emanating from either side of the 2D film, so that the resulting field decays exponentially in each semi-infinite vacuum region; for bilayer systems, we further incorporate a field in the central region that is the combination of two evanescent waves internally emanating from the two films; the amplitudes of all waves are determined from the customary boundary conditions imposed from Maxwell's equations, defining a homogeneous linear system of equations that has a solution only for vanishing values of the secular determinant; this leads to the sought-after dispersion relation between q and ω . For single-layer systems, the resulting dispersion relation of 2D plasmons reduces to $q_z = -2/\chi_L(q, \omega)$, where $q_z = \sqrt{q^2 - k_0^2}$. For bilayer structures, a low-frequency solution of acoustic plasmons arises from the antisymmetric coupling of the plasmon modes of the two films, namely, $q_z \chi_L(q, \omega) = -2/(1 - e^{-q_z d})$. In our calculations, the electric susceptibility $\chi_L(q, \omega)$ in Eq. (3) is used for 2DEGs (Fig. 3 a,b), while for graphene systems (Fig. 3c-f) the electric susceptibility corresponding to this material is adopted. Finally, we define the effective refractive index as $n_{\text{eff}}(\omega) = qc/\omega$ (Fig. 3a-c).

EM momentum in 2D plasmons. In the free standing 2D systems considered in Fig. 3, the field is entirely distributed in the vacuum, where the momentum density is unambiguously given by $E_y(r)H_z(r)/2c^2$. The field distribution is simultaneously obtained when solving the dispersion as indicated above. For single-layer systems, the field decays exponentially in the vacuum on either side, so direct integrating along \hat{z} leads to $g_{\text{EM}} = \omega \varepsilon_0 q |E_x|^2 / 2q_z^3 c^2$, where E_x is the field amplitude on the plane of the 2D system. A similar procedure for bilayer systems involves integration over the intermediate region, leading to

$$g_{\text{EM}} = \frac{\omega \varepsilon_0 q}{2q_z^3 c^2} \left[1 + \frac{2e^{-q_z d} q_z d + 1 - e^{-2q_z d}}{(1 - e^{-q_z d})^2} \right] |E_x|^2.$$

Acknowledgements This work has been supported in part by the Spanish MINECO (Grants No. MAT2017-88492-R and No. SEV2015-0522), ERC (Advanced Grant No. 789104-eNANO), the Catalan CERCA Program, and Fundació Privada Cellex.

References

1. Minkowski, H. Die Grundgleichungen für die elektromagnetischen Vorgänge in bewegten Körpern. *Nachr. Ges. Wiss. Göttin Math.-Phys. Kl.* **1908**, 53–111 (1908).
2. Abraham, M. Zur elektrodynamik bewegter körper. *Rend. Circ. Mat. Palermo* **28**, 1–28 (1909).
3. Einstein, A. & Laub, J. Zur elektrodynamik bewegter körper. *Ann. der Phys.* **331**, 541–550 (1908).
4. Abraham, M. Sull'ellettrodinamica di Minkowski. *Rend. Circ. Mat. Palermo* **30**, 33–46 (1910).
5. Shockley, W. A “try simplest cases” resolution of the Abraham-Minkowski controversy on electromagnetic momentum in matter. *Proc. Natl. Acad. Sci. USA.* **60**, 807 (1968).
6. Gordon, J. P. Radiation forces and momenta in dielectric media. *Phys. Rev. A* **8**, 14 (1973).
7. Nelson, D. F. Momentum, pseudomomentum, and wave momentum: Toward resolving the Minkowski-Abraham controversy. *Phys. Rev. A* **44**, 3985 (1991).
8. Leonhardt, U. Optics: Momentum in an uncertain light. *Nature* **444**, 823 (2006).
9. Pfeifer, R. N. C., Nieminen, T. A., Heckenberg, N. R., & Rubinsztein-Dunlop, H. Colloquium: Momentum of an electromagnetic wave in dielectric media. *Rev. Mod. Phys.* **79**, 1197 (2007).
10. Barnett, S. M. Resolution of the Abraham-Minkowski dilemma. *Phys. Rev. Lett.* **104**, 070401 (2010).
11. Milonni, P. W., & Boyd, R. W. Momentum of light in a dielectric medium. *Adv. Opt. Photon.* **2**, 519–553 (2010).

12. Mansuripur, M. Resolution of the Abraham–Minkowski controversy. *Opt. Commun.* **283**, 1997–2005 (2010).
13. Partanen, M., Häyrynen, T., Oksanen, J., & Tulkki, J. Photon mass drag and the momentum of light in a medium. *Phys. Rev. A* **95**, 063850 (2017).
14. Jones, R. V., & Richards, J. C. S. The pressure of radiation in a refracting medium. *Proc. R. Soc. Lond. A* **221**, 480–498 (1954).
15. Ashkin, A., & Dziedzic, J. M. Radiation pressure on a free liquid surface. *Phys. Rev. Lett.* **30**, 139 (1973).
16. Walker, G. B., & Lahoz, D. G. Experimental observation of Abraham force in a dielectric. *Nature* **253**, 339 (1975).
17. Walker, G. B., Lahoz, D. G., & Walker, G. Measurement of the Abraham force in a barium titanate specimen. *Can. J. Phys.* **53**, 2577–2586 (1975).
18. Jones, R. V., & Leslie, B. The measurement of optical radiation pressure in dispersive media. *Proc. R. Soc. Lond. A* **360**, 347–363 (1978).
19. Campbell, G. K. *et al.* Photon recoil momentum in dispersive media. *Phys. Rev. Lett.* **94**, 170403 (2005).
20. She, W., Yu, J., & Feng, R. Observation of a push force on the end face of a nanometer silica filament exerted by outgoing light. *Phys. Rev. Lett.* **101**, 243601 (2008).
21. Astrath, N. G. C., Malacarne, L. C., Baesso, M. L., Lukaszewicz, G. V. B. and Bialkowski, S. E. Unravelling the effects of radiation forces in water. *Phys. Rev. Lett.* **5**, 4363 (2014).
22. Gibson, A. F., Kimmitt, M. F., & Walker, A. C. Photon drag in germanium. *Appl. Phys. Lett.* **17**, 75–77 (1970).
23. Danishevskii, A. M., Kastal'skii, A. A., Ryvkin, S. M., & Yaroshetskii, I. D. Photon drag of free carriers in direct interband transitions in semiconductors. *Zh. Eksp. Teor. Fiz.* **58**, 544 (1970).
24. Luryi, S. Photon-drag effect in intersubband absorption by a two-dimensional electron gas. *Phys. Rev. Lett.* **58**, 2263 (1987).
25. Wieck, A. D., Sigg, H., & Ploog, K. Observation of resonant photon drag in a two-dimensional electron gas. *Phys. Rev. Lett.* **64**, 463 (1990).
26. Vengurlekar, A. S., & Ishihara, T. Surface plasmon enhanced photon drag in metal films. *Appl. Phys. Lett.* **87**, 091118 (2005).
27. Karch, J. *et al.* Dynamic Hall effect driven by circularly polarized light in a graphene layer. *Phys. Rev. Lett.* **105**, 227402 (2010).
28. Wooten, F. *Optical properties of solids* (Academic press, 2013).
29. Adler, S. L. Quantum theory of the dielectric constant in real solids. *Phys. Rev.* **126**, 413 (1962).
30. Boyd, R. W. *Nonlinear Optics* (Elsevier, 2008).
31. Kronig, R. D. L., & Penney, W. G. Quantum mechanics of electrons in crystal lattices. *Proc. R. Soc. Lond. A* **130**, 499–513
32. Jackson, J. D. *Classical Electrodynamics* Wiley (New York, 1999).
33. Hwang, E. H., & Sarma, S. D. Dielectric function, screening, and plasmons in two-dimensional graphene. *Phys. Rev. B* **75**, 205418 (2007).
34. Jablan, M., Buljan, H., & Soljačić, M. Shrinking light to allow forbidden transitions on the atomic scale. *Phys. Rev. B* **80**, 245435 (2009).
35. Chen, J. *et al.* Optical nano-imaging of gate-tunable graphene plasmons. *Nature* **487**, 77 (2012).
36. Fei, Z. *et al.* Gate-tuning of graphene plasmons revealed by infrared nano-imaging. *Nature* **487**, 82 (2012).
37. Rivera, N., Kaminer, I., Zhen, B., Joannopoulos, J. D., & Soljačić, M. Shrinking light to allow forbidden transitions on the atomic scale. *Science* **353**, 263–269 (2016).
38. Lundeberg, M. B. *et al.* Tuning quantum nonlocal effects in graphene plasmonics. *Science* **357**, 187–191 (2017).
39. Iranzo, D. A. *et al.* Probing the ultimate plasmon confinement limits with a van der Waals heterostructure. *Science* **360**, 291–295 (2018).

40. Economou, E. N. Surface plasmons in thin films. *Phys. Rev.* **182**, 539 (1969).
41. Diaconescu, B. *et al.* Low-energy acoustic plasmons at metal surfaces. *Nature* **448**, 57 (2007).